JOURNAL OF THEORETICAL
AND APPLIED MECHANICS
3, 38, 2000

FINITE ELEMENT ANALYSIS AND DESIGN OF PIEZOELECTRIC CONTROLLED SMART STRUCTURES

HARALD BERGER
ULRICH GABBERT
HEINZ KÖPPE
FALKO SEEGER

Otto-von-Guericke-Universität Magdeburg, Institut für Mechanik
e-mail: ulrich.gabert@mb.uni-magdeburg.de

The paper gives an overview of about recent developments in modeling, numerical analysis and design of piezoelectric controlled smart structures. Then, the theoretical basis of a general purpose finite element simulation tool developed by the authors is presented. This tool contains a number of coupled thermo-electro-mechanical 1D, 2D, 3D as well as layered plate and shell finite elements for simulating controlled structures in static and dynamic applications, where also optimization algorithms (e.g. for actuator location) can be included. Finally, three examples; i.e., actively controlled beam, vibration isolation of a box, and vibration isolation of a plate as part of an excited cylinder structure, are presented to demonstrate the capability and efficiency of the simulation and design tool.

Key words: smart sructures, finite element analysis, piezoelasticity

1. Introduction

Over the past few years the smart structures concept has been given increasing attention in many branches of engineering and several novel engineering applications have been developed. Smart structures or to be more precise structronic (structure + electronic) systems are characterized by synergistic integration of active materials into a passive structure connected by a control system to enable automatic adaptation to changing environmental conditions. Piezoelectric materials (e.g. PZT, PVDF) as wafers and fibers are widely used as distributed sensors and actuators in smart structures, where especially hybrid composites (combination of fiber-reinforced angle-ply and piezoelectric

laminae) are very powerful smart material systems. Such hybrid composites are characterized by high structural conformity preventing major disturbances of mechanical behavior as a result of integration of the actuator and sensor materials into a structure. The active material forms an integral part of the load-bearing structure itself and does not cause any significant change in the passive behavior of the structure. On the other hand it offers a great potential for altering the structural response such that the structural behavior can adapt to new environment conditions or performance requirements, e.g. active shape control and active vibration damping. In comparison to the passive structures, new challenging tasks arise from the integration of smart materials as actuators or sensors into the base elastic structure. Today, possible fields of application of the structronic concept include mechanical engineering, aerospace engineering and civil engineering, manufacturing, transportation, robotics, information technology, medicine and many other branches.

The increasing engineering activities in the development and industrial applications of piezoelectric smart structures require effective and reliable simulation and design tools. Although the piezoelectric effect has been known for a long time (J. and P. Currie, 1880), its application to control systems is rather new (e.g. Tzou and Anderson, 1992). A number of classical textbooks describe the theoretical foundations of the piezoelectric effect as a coupled field problem (Voigt, 1910; Mason, 1954; Mindlin, 1961; Parkus, 1979; Nye, 1985) and analytical solutions have been developed to solve engineering problems (e.g. Tiersten, 1969; Tzou, 1993). However, more powerful calculation tools are required for the analysis and design process of complex engineering smart structures with integrated piezoelectric wafers and fibers as the actuators/sensors. Here, the Finite Element Method (FEM) provides an effective technique. Due to its wide-spread use it has become a theoretically and practically established method for a wide range of applications. It has also proved to be a suitable means for solving coupled piezoelectric field problems. Over the past few years significant progress has been made in the development of finite elements for coupled electromechanical fields (for an overview see Chee et al. (1998)), but most software developments and applications are still limited to simple cases, special element types and special numerical solution techniques (e.g. Ha et al., 1992; Hwang and Hyun, 1993; Tzou, 1993, 1994). Also in general purpose finite element codes, such as ABAQUS and ANSYS, only quadrilateral and hexahedron elements are available for the solution of coupled electromechanical fields (Lin et al., 1994). Therefore, our research group has concentrated on extending the existing finite element software, i.e. COSAR general purpose code, by adding a number of coupled electromechanical finite

elements which cover 1D, 2D, 3D and layered composite shell problems. An essentially new theoretical aspect was to include coupling between the electric, thermal and mechanical fields in the finite element software. In several applications of smart structures the influence exerted by temperature is important and has to be taken into account, e.g. in aerospace structures. Although some special finite element developments include the thermal effect, most frequently only temperature-induced deformations are taken into consideration (e.g. Tzou and Ye, 1994; Rao and Sunar, 1993; etc.). Our software comprises the fully coupled three field equations; however, the piezocaloric effect is rather small and can be neglected in most cases (Görnandt and Gabbert, 2000). Hence, the basic equations in this paper are given in a general manner, i.e. not considering a special finite element type, and do not include the direct coupling between the electromechanical and temperature fields. If required, this coupling can be taken into account iteratively. When applying our simulation software the parameters of the material tensors serve as input data and need to be established. In particular, in active composites controlled by thin piezoelectric fibers (Sporn and Schönecker, 1999), it is time-consuming and expensive to measure these macroscopic (homogenized) material data which are non-linear functions of the properties, arrangement and volume fraction of the constituents in the composite. Alternatively, analytical methods (e.g. based on the Mori-Tanaka-type mean field approach) as well as numerical methods (e.g. based on the finite element analysis of a representative volume element) can be employed to calculate homogenized material tensors of a heterogeneous material system (Gabbert et al., 1999b).

The smart structures finite element code developed is suited for solving problems in electroelasticity (static and dynamic), heat transfer and nonlinear mechanics on the basis of a large library of finite element types, a collection of numerical solution techniques, and of course comprehensive pre- and post-processing procedures. The code provides the option to use finite elements with a variable number of degrees of freedom (DOF) at nodes. The coupled electromechanical finite elements were developed by adding the electric potential as new DOFs to the nodes. Also graphical features, e.g. description of the material properties, application of electric loads, graphical representation of electric field values, etc., were added to provide a user-friendly simulation and design software. In addition, some modifications to the numerical solution algorithms were required as, for instance, the stiffness matrices for coupled electromechanical fields are generally not positive definite. Furthermore, the finite element code also includes a substructure technique. It contains simple control algorithms, but also a specialised data interface to special control design tools, such as Matlab/Simulink.

2. Basic equations of piezoelasticity

The coupled electromechanical behavior of a polarizable (but not magnetizable) piezoelectric smart material can be modeled with a sufficient accuracy by means of linearized constitutive equations. These linear equations can be derived from the energy expression (Tiersten, 1969) in a quadratic form of the primary field variables, i.e. mechanical strain $\boldsymbol{\varepsilon}$ and electric field $\mathbf{E}$, on the assumption that the temperature distribution θ is *a priori* known or can be calculated independently of the electromechanical fields. After Tiersten (1969) and Parkus (1970) the potential function can be written in the form

$$H(\boldsymbol{\varepsilon}, \mathbf{E}) = \frac{1}{2}\boldsymbol{\varepsilon}^{\top}\mathbf{C}\boldsymbol{\varepsilon} - \boldsymbol{\varepsilon}^{\top}\mathbf{e}\mathbf{E} - \frac{1}{2}\mathbf{E}^{\top}\boldsymbol{\kappa}\mathbf{E} - \boldsymbol{\varepsilon}^{\top}\boldsymbol{\zeta}\bar{\theta} + \mathbf{E}^{\top}\boldsymbol{\pi}\bar{\theta} \tag{2.1}$$

from which the dependent variables; i.e., the mechanical stress $\boldsymbol{\sigma}$, and the electric displacement $\mathbf{D}$ are derived by partial differentiation as

$$\begin{aligned} \boldsymbol{\sigma} &= \frac{\partial H}{\partial \boldsymbol{\varepsilon}} = \mathbf{C}\boldsymbol{\varepsilon} - \mathbf{e}\mathbf{E} - \boldsymbol{\zeta}\bar{\theta} \\ \mathbf{D} &= -\frac{\partial H}{\partial \mathbf{E}} = \mathbf{e}^{\top}\boldsymbol{\varepsilon} + \boldsymbol{\kappa}\mathbf{E} + \boldsymbol{\pi}\bar{\theta} \end{aligned} \tag{2.2}$$

In matrix notation these equations can be written as

$$\boldsymbol{\Psi} = \mathbf{J}\boldsymbol{\gamma} - \overline{\boldsymbol{\Theta}} \tag{2.3}$$

with

$$\begin{aligned} \boldsymbol{\Psi} &= \begin{bmatrix} \boldsymbol{\sigma} \\ \mathbf{D} \end{bmatrix} & \mathbf{J} &= \begin{bmatrix} \mathbf{C} & \mathbf{e} \\ \mathbf{e}^{\top} & -\boldsymbol{\kappa} \end{bmatrix} \\ \boldsymbol{\gamma} &= \begin{bmatrix} \boldsymbol{\varepsilon} \\ -\mathbf{E} \end{bmatrix} & \overline{\boldsymbol{\Theta}} &= \begin{bmatrix} \boldsymbol{\zeta}\bar{\theta} \\ -\boldsymbol{\pi}\bar{\theta} \end{bmatrix} \end{aligned} \tag{2.4}$$

and the stress vector $\boldsymbol{\sigma}^{\top} = [\sigma_{11}, \sigma_{22}, \sigma_{33}, \sigma_{12}, \sigma_{23}, \sigma_{31}]$, the symmetric 6×6 elasticity matrix $\mathbf{C}$, the strain vector $\boldsymbol{\varepsilon}^{\top} = [\varepsilon_{11}, \varepsilon_{22}, \varepsilon_{33}, \varepsilon_{12}, \varepsilon_{23}, \varepsilon_{31}]$, the 6×3 piezoelectric matrix $\mathbf{e}$, the electric field vector $\mathbf{E}^{\top} = [E_1, E_2, E_3]$, the vector of thermal stress coefficients $\boldsymbol{\zeta}$, the temperature variation $\bar{\theta}$ of the body with respect to the initial temperature, the vector of electric displacements $\mathbf{D}^{\top} = [D_1, D_2, D_3]$, , the symmetric 3×3 dielectric matrix $\boldsymbol{\kappa}$, and the vector of pyroelectric coefficients $\boldsymbol{\pi}$. In general there are 21 independent elastic

constants, 18 piezoelectric constants, 6 dielectric constants, 6 thermal stress constants and 3 pyroelectric constants. In order to solve piezoelastic problems, it is essential to know these material coefficients (Nye, 1985; Tiersten, 1969). In a preliminary polarized ferroelectric ceramic, poled in direction 3 of a Cartesian coordinate system, the material behavior is transversal- isotropic and the number of material data is reduced to 5 elastic constants, 3 electric constants and 2 dielectric constants, which can be written as

$$\mathbf{C} = \begin{bmatrix} c_{11} & c_{12} & c_{13} & \cdot & \cdot & \cdot \\ & c_{11} & c_{13} & \cdot & \cdot & \cdot \\ & & c_{33} & \cdot & \cdot & \cdot \\ & & & c_{44} & \cdot & \cdot \\ & \text{symmetric} & & & c_{44} & \cdot \\ & & & & & \frac{1}{2}(c_{11}-c_{12}) \end{bmatrix} \tag{2.5}$$

$$\mathbf{e} = \begin{bmatrix} \cdot & \cdot & e_{31} \\ \cdot & \cdot & e_{31} \\ \cdot & \cdot & e_{33} \\ \cdot & e_{15} & \cdot \\ \cdot & e_{15} & \cdot \\ \cdot & 0 & \cdot \end{bmatrix} \qquad \boldsymbol{\kappa} = \begin{bmatrix} \kappa_{11} & \cdot & \cdot \\ \cdot & \kappa_{11} & \cdot \\ \cdot & \cdot & \kappa_{33} \end{bmatrix}$$

where the five independent elastic constants are measured under constant (or vanishing) electric field, while the three piezoelectric constants and the two dielectric constants are measured under constant (or vanishing) deformation. Materials of this type of symmetry are important due to their high piezoelectric coupling factor.

The linear constitutive relations of Eqs (2.3) are an approximation of the real non-linear behavior, which is quite accurate in low electric field applications, and gives sufficient results in most design processes of engineering smart structures. It should be mentioned here that in engineering applications a small non-linearity can be compensated for by a robust control algorithm, or by including an inverse model of the hysteresis loop in order to linearize the behavior, e.g. in the form of Preisach model or Buoc model (Kolsch, 1993). There are also non-linear models facilitating simulation of the poling process. However, due to the paper limitation this will not be discussed here.

The constitutive equations (2.3) together with the mechanical and electric balance equations as well as the mechanical and electric boundary conditions constitute a unique set of equations for the coupled electromechanical problem.

These are the three equations of motion written in matrix notation as

$$\mathbf{L}_u^{\top}\boldsymbol{\sigma} + \bar{\boldsymbol{p}} - \rho\ddot{\boldsymbol{u}} = \mathbf{0} \qquad \text{in } V \tag{2.6}$$

and the charge equation of electrostatics resulting from Maxwell's equations (Tiersten, 1969)

$$\mathbf{L}_\phi^{\top}\mathbf{D} = \mathbf{0} \qquad \text{in } V \tag{2.7}$$

where $\bar{\boldsymbol{p}}^{\top} = [\bar{p}_1, \bar{p}_2, \bar{p}_3]$ is the body force vector, $\boldsymbol{u}^{\top} = [u_1, u_2, u_3]$ is the vector of mechanical displacements described in a Cartesian coordinate system $\boldsymbol{x}^{\top} = [x_1, x_2, x_3]$, ρ is the mass density, and the two differentiation matrices $\mathbf{L}_u$ and $\mathbf{L}_\phi$ are

$$\mathbf{L}_u^{\top} = \begin{bmatrix} \dfrac{\partial}{\partial x_1} & 0 & 0 & \dfrac{\partial}{\partial x_2} & 0 & \dfrac{\partial}{\partial x_3} \\ 0 & \dfrac{\partial}{\partial x_2} & 0 & \dfrac{\partial}{\partial x_1} & \dfrac{\partial}{\partial x_3} & 0 \\ 0 & 0 & \dfrac{\partial}{\partial x_3} & 0 & \dfrac{\partial}{\partial x_2} & \dfrac{\partial}{\partial x_1} \end{bmatrix} \qquad \mathbf{L}_\phi = \begin{bmatrix} \dfrac{\partial}{\partial x_1} \\ \dfrac{\partial}{\partial x_2} \\ \dfrac{\partial}{\partial x_3} \end{bmatrix} \tag{2.8}$$

With $\mathbf{L}_u$ and $\mathbf{L}_\phi$ the balance equations (2.6) and (2.7) can be written in a compact form as

$$\mathbf{L}^{\top}\boldsymbol{\Psi} + \bar{\boldsymbol{b}} - \boldsymbol{\rho}\ddot{\boldsymbol{q}} = \mathbf{0} \tag{2.9}$$

where $\mathbf{L}$, $\bar{\boldsymbol{p}}$, ρ and $\boldsymbol{q}$ are

$$\mathbf{L} = \begin{bmatrix} \mathbf{L}_u & \mathbf{0} \\ \mathbf{0} & \mathbf{L}_\phi \end{bmatrix} \qquad \bar{\boldsymbol{b}} = \begin{bmatrix} \bar{\boldsymbol{p}} \\ 0 \end{bmatrix} \qquad \boldsymbol{\rho} = \begin{bmatrix} \rho\mathbf{I} & \mathbf{0} \\ \mathbf{0} & 0 \end{bmatrix} \qquad \ddot{\boldsymbol{q}} = \begin{bmatrix} \boldsymbol{u} \\ \phi \end{bmatrix} \tag{2.10}$$

In the following we use the linear strain-displacement relation $\boldsymbol{\varepsilon} = \mathbf{L}_u\boldsymbol{u}$ and the relation between the electric field vector $\mathbf{E}$ and electric potential ϕ in form of $\mathbf{E} = -\mathbf{L}_\phi\phi$. These two equations can be written as

$$\boldsymbol{\gamma} = \begin{bmatrix} \boldsymbol{\varepsilon} \\ -\mathbf{E} \end{bmatrix} = \mathbf{L}\boldsymbol{q} \tag{2.11}$$

With Eq (2.11) the constitutive relation (2.3) can be rewritten as

$$\boldsymbol{\Psi} = \mathbf{J}\mathbf{L}\boldsymbol{q} - \bar{\boldsymbol{\Theta}} = \mathbf{0} \tag{2.12}$$

With Eq (2.12) the balance equations (2.9) can be written as

$$\mathbf{L}^{\top}\mathbf{J}\mathbf{L}\boldsymbol{q} - \mathbf{L}^{\top}\bar{\boldsymbol{\Theta}} + \bar{\boldsymbol{b}} - \boldsymbol{\rho}\ddot{\boldsymbol{q}} = \mathbf{0} \tag{2.13}$$

or in the extended form

$$\begin{bmatrix} \mathbf{L}_u^\top \mathbf{C} \mathbf{L}_u & \mathbf{L}_u^\top \mathbf{e} \mathbf{L}_\phi \\ \mathbf{L}_\phi^\top \mathbf{e}^\top \mathbf{L}_u & -\mathbf{L}_\phi^\top \boldsymbol{\kappa} \mathbf{L}_\phi \end{bmatrix} \begin{bmatrix} \boldsymbol{u} \\ \phi \end{bmatrix} - \begin{bmatrix} \mathbf{L}_u^\top \boldsymbol{\zeta} \bar{\theta} \\ -\mathbf{L}_\phi^\top \boldsymbol{\pi} \bar{\theta} \end{bmatrix} + \begin{bmatrix} \bar{\boldsymbol{p}} \\ 0 \end{bmatrix} - \begin{bmatrix} \rho \mathbf{I} & \mathbf{0} \\ 0 & 0 \end{bmatrix} \begin{bmatrix} \ddot{\boldsymbol{u}} \\ \ddot{\phi} \end{bmatrix} = \mathbf{0} \tag{2.14}$$

The mechanical stress and electric charge boundary conditions are

$$\bar{\boldsymbol{\tau}} - \boldsymbol{\tau} = \begin{bmatrix} \bar{\boldsymbol{t}} \\ \overline{Q} \end{bmatrix} - \mathbf{n} \boldsymbol{\Psi} = \mathbf{0} \qquad \text{on } O_\psi \tag{2.15}$$

where $\bar{\boldsymbol{t}}$ is the prescribed traction vector, $\overline{Q}$ is the surface charge, and $\mathbf{n}$ is a matrix of direction cosines which transforms the stresses and electric displacements to the coordinate system normal to the surface. Overbar means prescribed values at a particular part of the surface. The boundary conditions of mechanical displacements and electric potential are

$$\bar{\boldsymbol{q}} - \boldsymbol{q} = \mathbf{0} \qquad \text{on } O_q \tag{2.16}$$

In terms of the weighted residual method, a coupled electromechanical functional is provided by multiplying the balance Eqs (14) with the vector $\delta \boldsymbol{q}^\top = [\delta \boldsymbol{u}^\top, \delta \phi]$ containing the virtual displacement $\delta \boldsymbol{u}$ and virtual electric potential $\delta \phi$, respectively, and integrating over the entire domain. This results in

$$\delta \boldsymbol{\chi} = \int_V \delta \boldsymbol{q}^\top (\mathbf{L}^\top \mathbf{J} \mathbf{L} \boldsymbol{q} - \mathbf{L}^\top \overline{\boldsymbol{\Theta}} + \bar{\boldsymbol{b}} - \boldsymbol{\rho} \ddot{\boldsymbol{u}}) \, dV + \int_{O_t} \delta \boldsymbol{q}^\top (\bar{\boldsymbol{\tau}} - \boldsymbol{\tau}) \, dO = \mathbf{0} \tag{2.17}$$

It is assumed that the virtual quantities are admissible, and consequently, fulfil the boundary conditions (2.16). Using partial integration and the Gaussian integral theorem, the following form of the functional can be derived from Eqs (2.17)

$$\begin{aligned} \delta \boldsymbol{\chi} \;=\; & -\int_{V_c} \delta \boldsymbol{q}^\top \boldsymbol{\rho} \ddot{\boldsymbol{u}} \, dV - \int_{V_c} (\mathbf{L} \delta \boldsymbol{q})^\top \mathbf{J} \mathbf{L} \boldsymbol{q} \, dV + \int_{V_c} \delta \boldsymbol{q}^\top \bar{\boldsymbol{b}} \, dV + \\ & + \int_{V_c} (\mathbf{L} \delta \boldsymbol{q})^\top \overline{\boldsymbol{\Theta}} \, dV + \int_{O_t} \delta \boldsymbol{q}^\top \bar{\boldsymbol{\tau}} \, dO = \mathbf{0} \end{aligned} \tag{2.18}$$

This formulation creates a suitable basis for the development of any type of finite element for coupled electromechanical field problems.

3. Finite element analysis of piezomechanical problems

In each finite element the unknown field variables, mechanical displacements u_i and electric potential ϕ, are approximated by shape functions $N_k^{(u)}(\boldsymbol{x})$ and $N_k^{(\phi)}(\boldsymbol{x})$ as

$$u_i(\boldsymbol{x},t) = \sum_{(k)} N_k^{(u)}(\boldsymbol{x}) u_{ik}(t) \qquad \phi(\boldsymbol{x},t) = \sum_{(k)} N_k^{(\phi)}(\boldsymbol{x}) \phi_k(t) \tag{3.1}$$

where u_{ik} and ϕ_k are the time-dependent unknown nodal values of the element approximate function. In the matrix form these equations can be written as

$$\boldsymbol{q}(\boldsymbol{x},t) = \mathsf{N}(\boldsymbol{x}) \boldsymbol{q}_e(t) \tag{3.2}$$

with

$$\mathsf{N}(\boldsymbol{x}) = \begin{bmatrix} \mathsf{N}^{(u)} & \mathsf{0} \\ \mathsf{0} & \mathsf{N}^{(\phi)} \end{bmatrix} \qquad \boldsymbol{q}_e = \begin{bmatrix} \boldsymbol{u}_e \\ \phi_e \end{bmatrix} \tag{3.3}$$

where $\mathsf{N}^{(u)}$ and $\mathsf{N}^{(\phi)}$ are the mechanical and electric shape function matrices, and the vector $\boldsymbol{q}_e$ contains the mechanical and electric element nodal degrees of freedom $\boldsymbol{u}_e$ and ϕ_e, respectively. Application of the differentiation matrix L to $\boldsymbol{q}$ results in

$$\mathsf{L}\boldsymbol{q} = \mathsf{L}\mathsf{N}\boldsymbol{q}_e = \mathsf{B}\boldsymbol{q}_e \tag{3.4}$$

with

$$\mathsf{B} = \mathsf{L}\mathsf{N} = \begin{bmatrix} \mathsf{L}_u \mathsf{N}^{(u)} & \mathsf{0} \\ \mathsf{0} & \mathsf{L}_\phi \mathsf{N}^{(\phi)} \end{bmatrix} \tag{3.5}$$

Introducing the approximate function appearing in Eq (3.2) into Eq (2.18) and taking into account Eq (3.4) as well as $\mathsf{L}\delta\boldsymbol{q} = \mathsf{L}\mathsf{N}\delta\boldsymbol{q}_e = \mathsf{B}\delta\boldsymbol{q}_e$ we get

$$\delta\boldsymbol{q}_e^{\top}(\mathsf{M}_e\ddot{\boldsymbol{q}}_e + \mathsf{K}_e\boldsymbol{q}_e - \mathsf{F}_e) = 0 \tag{3.6}$$

If, in addition the velocity proportional damping $\mathsf{R}_e\dot{\boldsymbol{q}}_e$ is taken into account, from Eq (3.6) follows the semi-discrete form of equation of motion of a coupled electromechanical problem as

$$\mathsf{M}_e\ddot{\boldsymbol{q}}_e + \mathsf{R}_e\dot{\boldsymbol{q}}_e + \mathsf{K}_e\boldsymbol{q}_e = \mathsf{F}_e \tag{3.7}$$

The mass matrix M_e, generalized stiffness matrix K_e and generalized force vector $\boldsymbol{F}_e$ of an element (e) are

$$\mathbf{M}_e = \int_{V_e} \mathbf{N}^\top \boldsymbol{\rho} \mathbf{N}^\top \, dV \qquad \mathbf{K}_e = \int_{V_e} \mathbf{B}^\top \mathbf{J} \mathbf{B}^\top \, dV$$
$$\mathbf{F}_e = \int_{V_e} \mathbf{N}^\top \bar{\boldsymbol{b}} \, dV + \int_{V_e} \mathbf{B}^\top \overline{\boldsymbol{\Theta}} \, dV + \int_{O_e} \mathbf{N}^\top \bar{\boldsymbol{\tau}} \, dO \tag{3.8}$$

Based on the above theoretical background, a library of piezoelectric finite elements was developed. In the following the paper presents some of these developments and describes the status of the finite element software developed for electromechanical problems.

4. Simulation and design software

4.1. Finite element library

The finite element library for piezoelectric controlled smart structures (see Fig.1) developed on the basis of the above given equations, includes solid elements, plane elements, axisymmetric elements, rod elements as well as special multilayer composite shell elements (see Berger et al., 1998). The shape functions of the finite elements can be linear or quadratic and the isoparametric element concept was used to approximate the element geometry. The solid element family consists of a basic brick-type element (hexahedron) and some special degenerated elements derived by collapsing nodes. The quadrilateral and triangular multilayered shell elements shown in Fig.1 were developed basing on the triangular piezoelectric shell element presented by Tzou and Ye (1994). The element presented by Tzou and Ye is based on a discrete layer theory in orthogonal curvilinear co-ordinates. However, this restricts application of the element to structures with uniform curvature (planes, cylinders, cones, hemispheres, etc.). We added a quadrilateral element and extended the geometry approximation by an isoparametric description. These new elements permit modelling of laminated structures. The electromechanical behavior of each layer is separately approximated by shape functions of different polynomial degrees in each direction, and each layer can be either active or passive (see Köppe et al., 1998). A linear approximation of the displacements in normal direction to each layer is used, and consequently, the element corresponds to the classical discrete layer theory. The element family is more efficient compared to

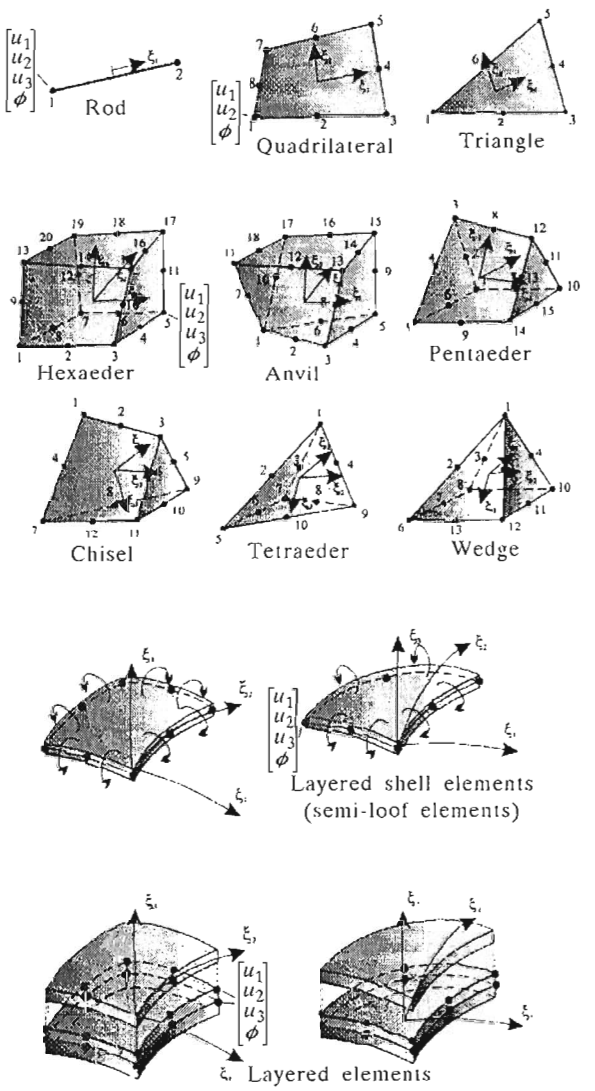

Fig. 1. Piezoelectric finite elemnt library of COSAR

the conventional isoparametric hexahedron elements. Thin shell assumptions can be included for the shell as a whole or several layers, and consequently the number of degrees of freedom can be reduced by constraints. These elements also facilitate effective investigations into the global and local effects, such as the transition behavior of active to passive parts of a structure or delamination propagation (Cao et al., 1998). Recently, we extended the finite element library by quadrilateral and triangular curved thin shell composite elements based on the classical Kirchhoff-Love hypothesis, where different approximations of the electromechanical coupling are included:

- Electric influence is taken into account in terms of distributed forces and moments
- Difference of the electric potential of each active layer is taken into account as an additional degree of freedom of the element (poling in normal direction)
- Each element node has as many additional electric degrees of freedom as there are active layers in the composite (in-plane electric poling).

These elements were developed on the basis of classical *SemiLoof* shell-type elements (Irons, 1976). The test results demonstrate that in thin shell structures these elements provide sufficient accuracy in modeling the global structural behavior at a drastically reduced number of degrees of freedom.

4.2. Numerical solution

For static solutions a special optimized submatrix-oriented Cholesky solver was developed taking into consideration that, in general, the stiffness matrix $\mathbf{K}$ assembled from the element contributions is not positive definite. Only minor modifications to the original algorithm are required to decomposed $\mathbf{K}$ as $\mathbf{K} = \mathbf{R}^{\top}\mathbf{I}\mathbf{R}$ with $\mathbf{I} = \mathrm{diag}(\pm 1)$ depending on the sign of the diagonal term during decomposition. The solution is then calculated by forward substitution $\mathbf{R}^{\top}\mathbf{Z} = \mathbf{F}$ and backward substitution $\mathbf{R}\boldsymbol{q} = \mathbf{I}\mathbf{Z}$, which results in the solution $\boldsymbol{q}$.

For solving eigenvalue problems the subspace iteration method in the form proposed by McCormick and Noe is used. In transient problems modal based techniques as well as time integration schemes, such as Newmark-Method, Wilson-Method, or Central-Difference-Method, can be applied. It should be mentioned here that it is important to scale the matrix $\mathbf{J}$ in Eq (2.3) when using standard SI units in order to avoid extremely large differences in the coefficients of the generalized stiffness matrix $\mathbf{K}$, which cause numerical problems due to a very high condition number of the matrix. If a scaling parameter α

is introduced (e.g. $\alpha \approx 10^{10}$), the vector of nodal degrees of freedom, the material matrix $\mathbf{J}$ and the temperature vector $\overline{\boldsymbol{\Theta}}$ change to

$$\boldsymbol{q}_e = \begin{bmatrix} \boldsymbol{u}_e \\ \frac{1}{\alpha}\phi_e \end{bmatrix} \qquad \mathbf{J} = \begin{bmatrix} \mathbf{C} & \alpha\mathbf{e} \\ \alpha\mathbf{e}^\top & -\alpha^2\boldsymbol{\kappa} \end{bmatrix} \qquad \overline{\boldsymbol{\Theta}} = \begin{bmatrix} \boldsymbol{\zeta}\bar{\theta} \\ -\alpha\boldsymbol{\pi}\bar{\theta} \end{bmatrix} \tag{4.1}$$

which also has to be taken into account by prescribing electrical boundary conditions or during the simulation of controlled structures.

The finite element code is also capable of using a substructure technique facilitating the separation of mechanical and piezoelectric structural parts into different substructures to reduce the number of DOFs.

4.3. Sensing and control

Sensing and control of smart structures have become challenging tasks over the past decade and a great many papers have been published on this subject. Our finite element software is provided with a data interface to control design tools, such as Matlab/Simulink, to support the controller design for engineering applications and facilitate both the use of model reduction and model updating techniques. For directly incorporating of controllers into the finite element simulation tool some simple approaches have been implemented. If for instance the required actuator output voltage $\boldsymbol{q}_A$ is expressed by the sensor input signals $\boldsymbol{q}_S$, $\dot{\boldsymbol{q}}_S$ as

$$\boldsymbol{q}_A = \mathbf{Q}_P\boldsymbol{q}_S + \mathbf{Q}_D\dot{\boldsymbol{q}}_S \tag{4.2}$$

where the matrices $\mathbf{Q}_P$ and $\mathbf{Q}_D$ can be calculated by minimizing the quadratic cost functional of optimal control, Eq (4.2) can be simply incorporated into the equation of motion. In general, the result are non-symmetric generalized stiffness and damping matrices, which can be avoided by taking into account the influence of the actuators as a control force vector $\boldsymbol{F}_C$ on the right hand side of the equation of motion, which results in

$$\mathbf{M}\ddot{\boldsymbol{q}} + \mathbf{C}\dot{\boldsymbol{q}} + \mathbf{K}\boldsymbol{q} = \boldsymbol{F} + \boldsymbol{F}_C \tag{4.3}$$

From a numerical point of view this is more effective for the step by step time integration of the equation for which an iterative scheme can be used to ensure sufficient accuracy. In several cases more simple control laws with collocated actuator/sensor design, such as direct proportional feedback control or negative velocity feedback control, result in a good overall damping behavior.

5. Examples

5.1. Actively controlled beam

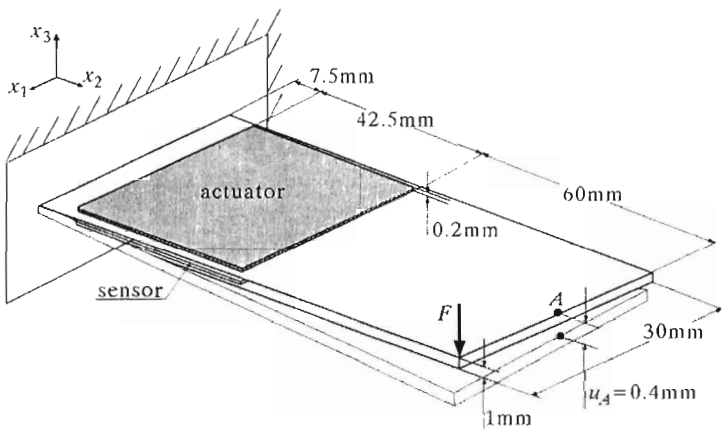

Fig. 2. Actively controlled beam

In Fig.2 the geometry of the beam is given, which is attached (glued) with a sensor and an actuator patch at the top and bottom surfaces, respectively, to actively control the beam. The material of the base beam structure is steel. The actuator and the sensor material is PIC151 (made by PI Ceramic Gmbh, Germany) with a thickness of 0.2 mm. In this example the time response was estimated, where as the initial condition a static deflection of the beam was used. This initial deformation of the beam is caused by a single load F at the tip of the beam (initial deformation of $u_A = 0.4\,\text{mm}$ at point A). The control by means of a simple feedback algorithm was realised, where the measured sensor signal (voltage) was amplified and fed back to the actuator. The finite element simulation was carried out using the electromechanical coupled hexahedron elements (see Fig.1). In Fig.3 the time displacement response of a point on the free end of beam is shown, and in Fig.4 the frequency response function of the beam tip is given. Fig.3 and Fig.4 demonstrate a good damping behavior if using this simple feedback control algorithm.

5.2. Vibration isolation of a box

A typical application in the field of vibration suppression is the protection of highly sensitive electronic devices against environmental disturbances. A numerical experiment was performed aiming at protecting a box containing

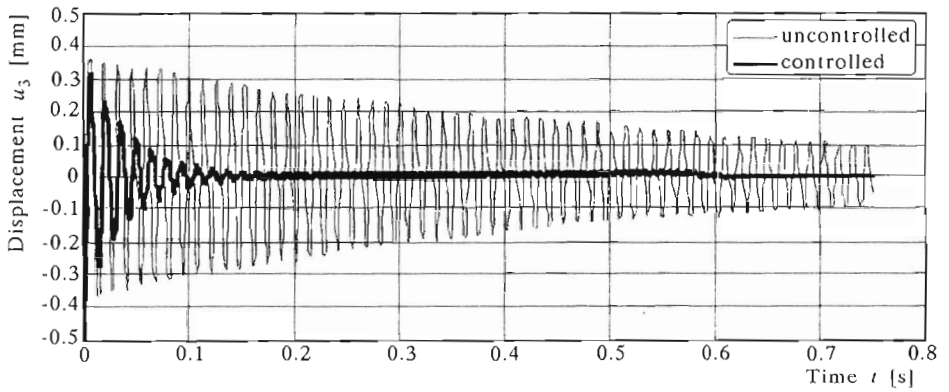

Fig. 3. Uncontrolled snd controlled responses of the beam tip

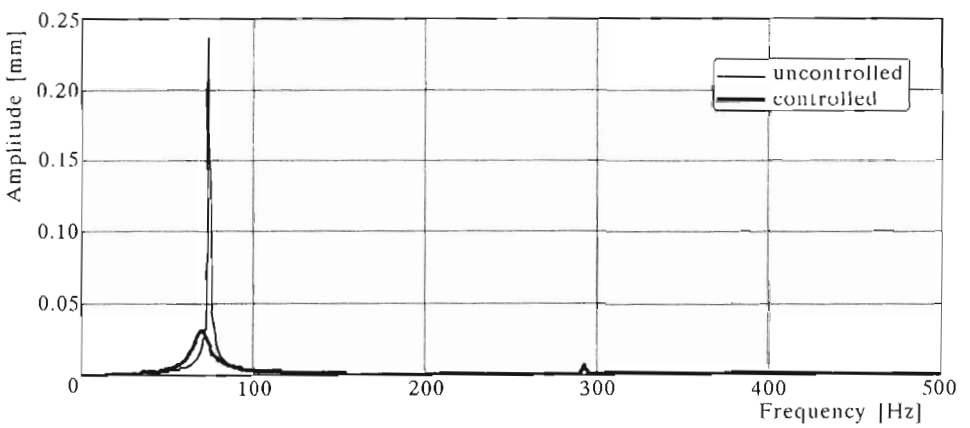

Fig. 4. Frequency response function of the beam tip

such electronic devices against any vibration by providing it with an active damping system. The box comprising two fairly stiff borders was fixed to a base frame by means of eight rods. The base frame was mounted to four rigid supports (Fig.5).

This structural system was designed in the way that it could be excited by different environmental disturbances (e.g. force excitation at any point, displacement excitation of the supports, etc.). To this end, four actively controllable rods (rods with integrated piezoelectric stack actuators) were mounted between the box and the supporting frame. The box, borders and base frame were modelled by means of eight-node thin *SemiLoof* shell elements (Fig.1) of different thicknesses. The chosen coarse finite element mesh reflects sufficiently

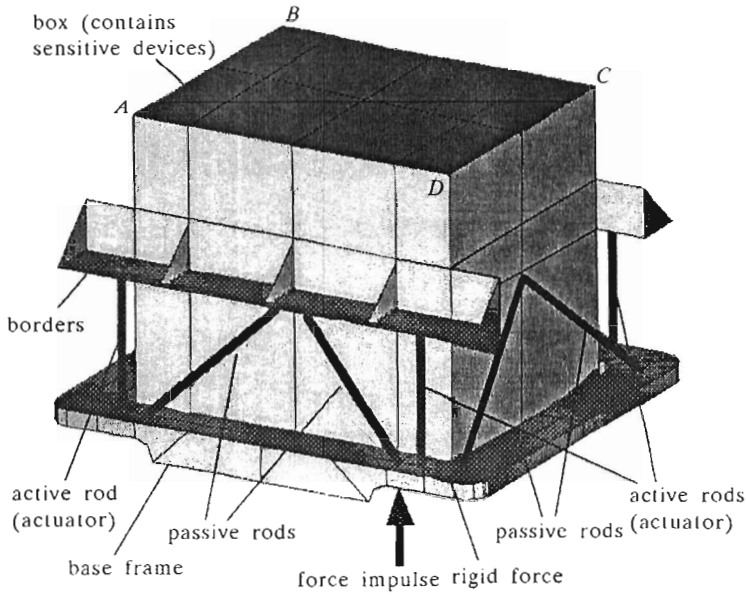

Fig. 5. Complete model of the box

the dynamic behavior of the system (Fig.6). The base frame, box and borders were made of aluminium. The passive rods were made of steel, and for the active rods commercially available piezoceramic stack actuators were used.

To study the principal dynamic behavior of the whole system the natural frequencies and corresponding natural modes were calculated. The first, third and fifth mode were nodding modes. The second mode was the vertical vibration and the fourth mode was the transversal vibration. Table 1 gives the natural frequencies for the first five modes.

Table 1. Natural frequencies of the box

Mode 1	Mode 2	Mode 3	Mode 4	Mode 5
253 Hz	290 Hz	306 Hz	422 Hz	513 Hz

The first and the second natural modes are depicted in Fig.6 where the deformed and undeformed meshes are plotted. In all the investigated modes main deformation occurred in the base frame, whereas the box including the borders appeared to be almost rigid. For controlling the structure, the displacements at the upper end of the stack actuators were used as sensor signals. In order to damp the box vibration, the vertical displacements at four measuring points were amplified by a gain factor to obtain the actuator output voltage of

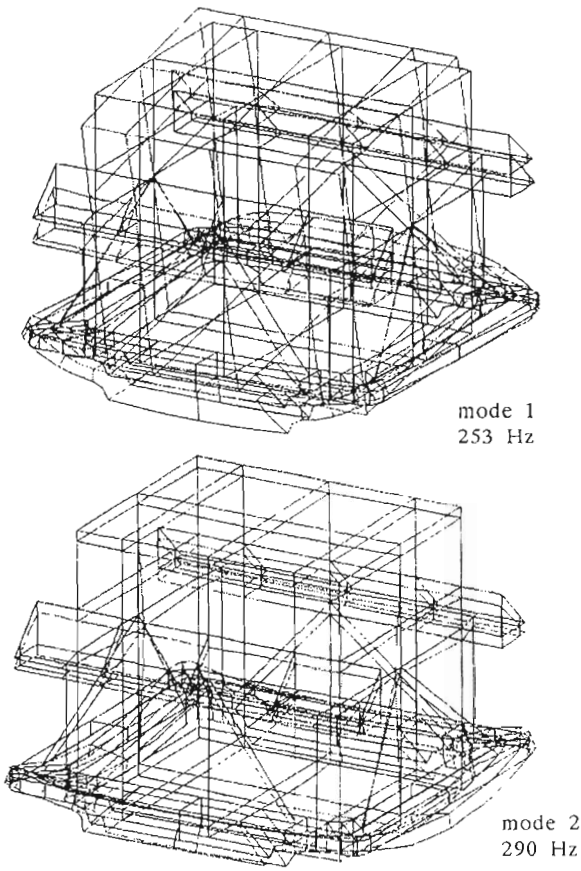

Fig. 6. Natural modes 1 and 2 of the box

active rods. As a control algorithm the collocated direct proportional feedback control method mentioned in Section 4.3 was used.

To study the principal damping behavior of the box with the active control mechanism, the system was subjected to an initial deflection corresponding to natural mode 1. The diagrams in Fig.7 show the uncontrolled and controlled deflections at the two representative points A and D (see Fig.5) on the upper surface of the box at a time interval of 0.1 s using two different gain factors (0.008 and 0.01) for control. The damping behavior observed was very good. In the further course of our investigation the base frame was excited by a force impulse shown in Fig.8 at a single point (see Fig.5). For estimating the damping behavior of the box the deflections at the four corner points A to D of the upper surface were considered. The diagrams in Fig.9 show the results

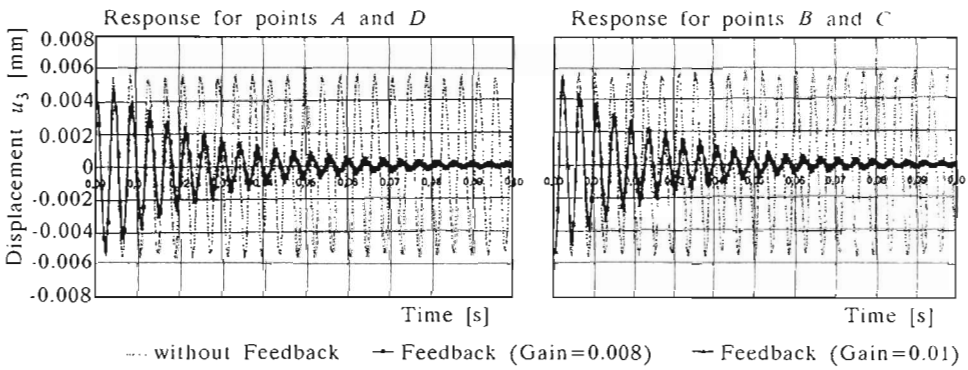

Fig. 7. Uncontrolled and controlled responses of the box (initial condition: deflection of the box in form of the first eigenmode)

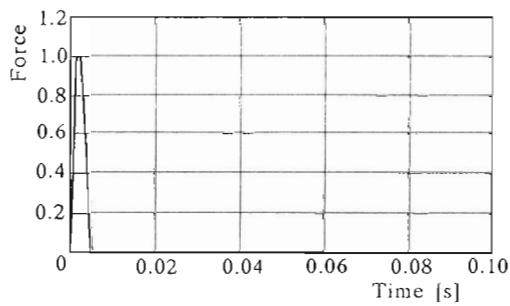

Fig. 8. Force impulse function (see Fig.5)

over a time interval of 0.1 s calculated with the gain factor of 0.01. Also in this case a good overall damping behavior can be seen. In Fig.10 the results obtained at the point A are transformed in the frequency domain, where the good damping behavior of the first two natural modes can be seen more clearly.

5.3. Vibration isolation of a plate as part of excited cylinder structure

The structure under consideration (Fig.11) consists of a composite cylinder with stringers and a base plate. The cylinder has a diameter and a length of 1000 mm. Actuators and sensors are placed at the bottom and top surfaces of the base plate in order to actively damp the plate structure. The cylinder and the stringers consist of CFK (Tenax HTA/LY 556, $\phi = 60\%$) with 8 layers of symmetric stacking sequence of $[90, -45, 45, 0, 0, 45, -45, 90]$ and a layer

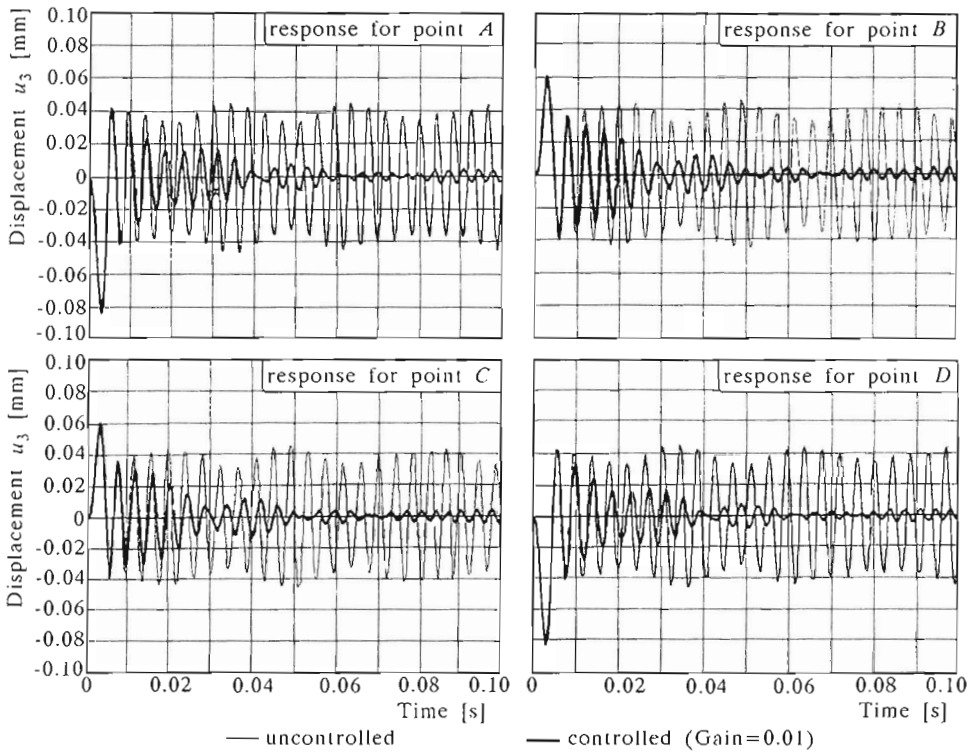

Fig. 9. Uncontrolled and controlled responses of the points $A \div D$ (exciting of the box by an force impulse)

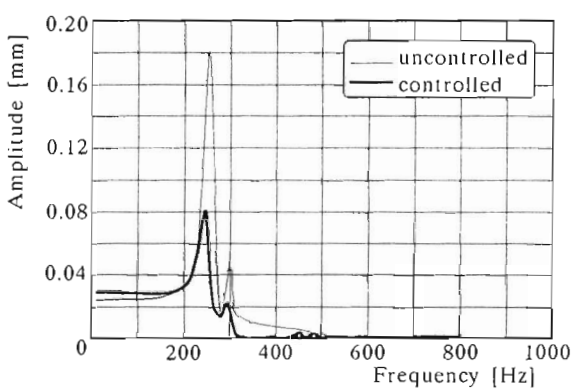

Fig. 10. Frequency response function of the point A (box excited by a force impulse)

thickness of 0.25 mm. Hence, the total thickness is 2 mm. The plate was built up with the same stacking sequence but with thin layers of 0.125 mm thickness. During the first numerical simulations the edge of the cylinder, the edge of the stringers and the edge of the base plate were clamped on the rear side (see Fig.11). The finite element model of the structure consists of 8-node active and passive *SemiLoof* shell elements, where each active element layer has an additional electric DOF.

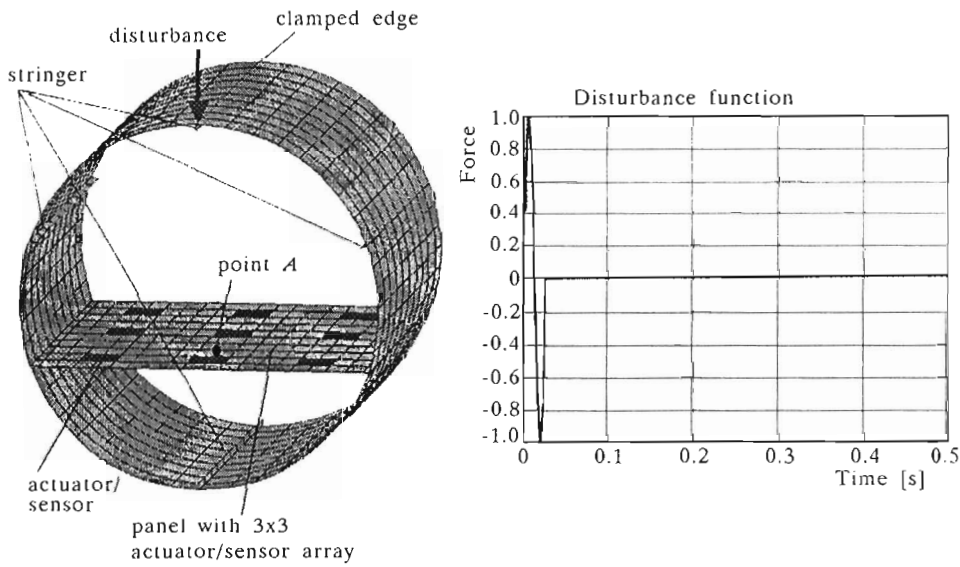

Fig. 11. Complete model of the cylinder structure, and force impulse function

This composite cylinder structure is used as a generic structure, which represents the complexity of, e.g., section of an aeroplane, train or car. Several experimental and numerical investigations are in progress to develop and to verify simulation and design tools, control and optimization strategies as well as experimental techniques to design real size structures.

In the first numerical study the vertical displacements of the panel should be damped actively by means of a collocated actuator and sensor design. Nine pairs of piezoelectric patches (wafers of PIC151 with the dimensions of $100 \times 100 \times 0.2$ mm) were arranged at the bottom and the top of the plate in a 3×3 array (Fig.11), where each of the nine pairs form a collocated actuator/sensor pair.

First, the voltage of each sensor patch at the top of the plate was amplified by a gain factor and simply fed back to the actuator patch. The structure was

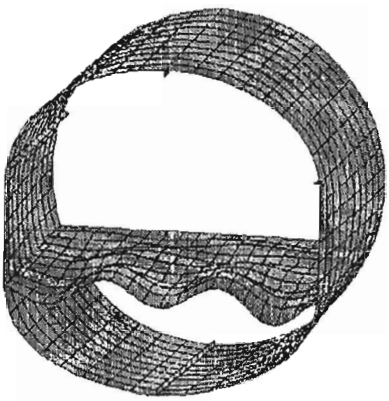

Fig. 12. Deformation of the cylinder the instant $t = 0.0135\,\mathrm{s}$

exited by a force impulse (position see Fig.11). Fig.12 shows the response of the structure after a time of $t = 0.0135\,\mathrm{s}$, in Fig.13 the response at the point A of the plate is given in the time domain, and in Fig.14 the frequency response function at the point A is shown. These results demonstrate that even with a very simple control strategy and the arrangement of actuators and sensors, which is of course not optimal for this case, a good damping behavior can be achieved. Of course, a better performance is possible with a better controller design as well as with an optimized actuator/sensor location (Weber et al., 1998).

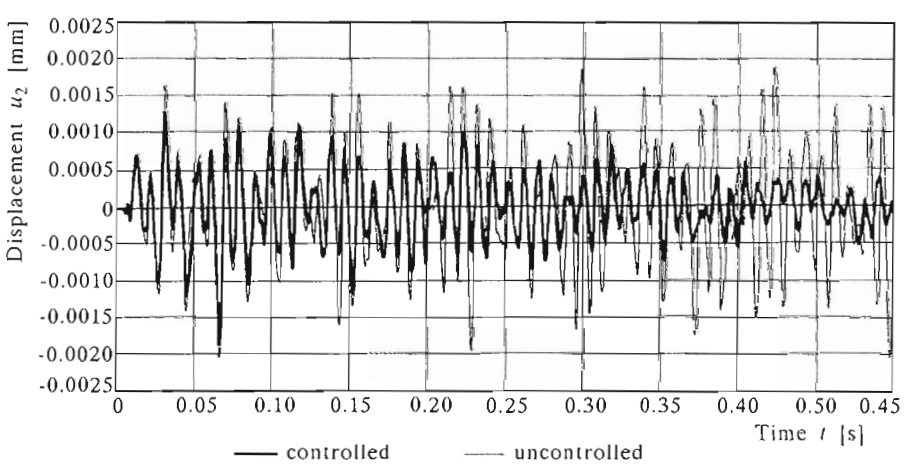

Fig. 13. Controlled and uncontrolled time responses of the point A

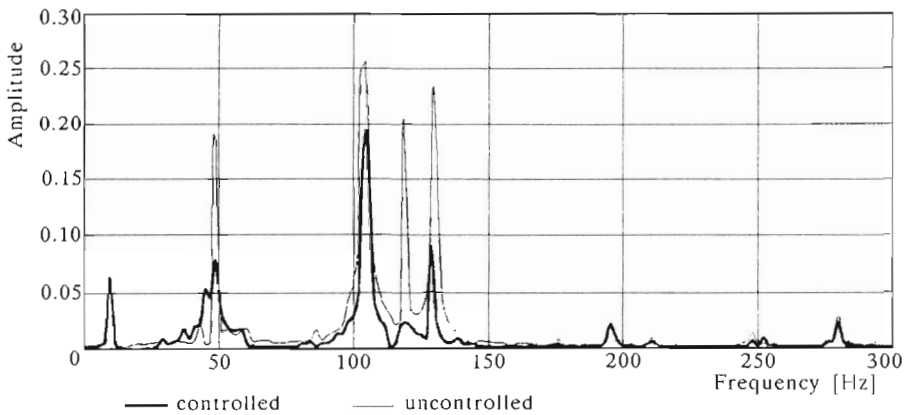

Fig. 14. Frequency responses function of the point A

6. Conclusion

The paper presents a general concept for a finite element based simulation and design tool of piezoelectric controlled smart structures. This tool enables the user to simulate both static and dynamic structural problems, including control as well as optimization of the actuator and sensor locations. Several benchmark examples were investigated to demonstrate the efficiency and accuracy of the simulation tool, and both analytical and experimental solutions were used to validate the results. The coupled electromechanical elements presented are also suitable to model local effects in adaptive materials, such as fracture, delamination, etc. Three examples; namely, actively controlled beam, vibration isolation of a box and vibration isolation of a plate as part of the excited cylinder structure – are presented to demonstrate the capability of the developed simulation and design tool.

Acknowledgement

This work was financially supported by the German Research Foundation (DFG) under the project number INK 25/B1-1 and by the German Ministry for Science and Technology (BMBF). This support is gratefully acknowledged.

References

1. BERGER H., CAO X., KÖPPE H., GABBERT U., 1998, Finite Element Based Analysis of Adaptive Structures, in *Fortschr.-Ber. VDI Reihe 11*, **268**, Düsseldorf, VDI Verlag, 103-114

2. CAO X., GABBERT U., POETZSCH R., 1998, Delamination Modelling and Analysis of Adaptive Composites, *Proceedings of the 39th AIAA Conference, Adaptive Structure Forum*, Long Beach, CA, paper AIAA-98-2046

3. CHEE C.Y., TONG L., STEVEN G.P., 1998, A Review on the Modelling of Piezoelectric Sensors and Actuators Incorporated in Intelligent Structures, *J. of Intelligent Material Systems and Structures*, **9**, 3-19

4. COSAR – General Purpose Finite Element Package: Manual, FEMCOS mbH Magdeburg (see also: http://www.femcos.de)

5. GABBERT U. (edit.), 1998, Modelling and Control of Adaptive Mechanical Structures, *Fortschr.-Ber. VDI Reihe 11*, **268**, Düsseldorf, VDI Verlag

6. GABBERT U., GÖRNANDT A., KÖPPE H., SEEGER F., 1999a, Benchmark Problems for the Analysis of Piezoelectric Controlled Smart Structures, *ASME, Design Engineering Technical Conferences DETC'99*, Las Vegas, Nevada, DETC99/VIB-8391

7. GABBERT U., KREHER W., KÖPPE H., 1999b, Mathematical Modeling and Numerical Simulation of Smart Structures Controlled by Piezoelectric Wafers and Fibers, *Proceedings of the EUROMAT'99 Conference*, Munich

8. GABBERT U., WEBER C-T., 1999, Analysis and Optimal Design of Piezoelectric Smart Structures by the Finite Element Method, *Proceedings of the European Conference on Computational Mechanics*, Munich

9. GÖRNANDT A., GABBERT U., 2000, Finite Element Analysis of Thermopiezoelectric Smart Strucures, *Acta Mechanica* (in submitted)

10. HA S.K., KEILERS C., CHANG F.-K., 1992, Finite Element Analysis of Composite Structures Containing Distributed Piezoceramic Sensors and Actuators, *AIAA Journal*, **30**, 3, 772-780

11. HWANG W.-S., HYUN C.P., 1993, Finite Element Modeling of Piezoelectric Sensors and Actuators, *AIAA Journal*, **31**, 5, 930-937

12. IRONS B.M., 1976, The Semiloof Shell Element, in Ashwell D.G. and Gallagher R.H. (edit.), *Finite Elements for Thin Shells and Curved Members*, J. Wiley, London

13. KOLSCH H., 1993, *Schwingungsdämpfung durch statische Hysterese*, VDI Verlag, Düsseldorf

14. KÖPPE H., GABBERT U., TZOU H.S., 1998, On Three-Dimensional Layered Shell Elements for the Simulation of Adaptive Structures, in *Fortschr.-Ber. VDI Reihe 11*, **268**, Düsseldorf, VDI Verlag, 103-114

15. LIN M.W., ABATAN A.O., ROGERS C.A., 1994, Application of Commercial Finite Element Codes for the Analysis of Induced Strain-Actuated Structures, *Proceedings of 2nd Int. Conference on Intelligent Materials*, Williamsburg (USA), 846-855

16. MASON W.P., 1954, *Piezoelectric Crystals and Their Application to Ultrasonics*, D. Van Nostrand Company, New York

17. MINDLIN R.D., 1961, On the Equations of Motion of Piezoelectic Crystals, in J.R.M. Radock (edit.), *Problems in Continuum Mechanics*, Society for Industrial and Applied Mathematics, Philadelphia, 282-290

18. NYE H.F., 1985, *Physical Properties of Crystals*, University Press, Oxford

19. PARKUS H. (edit.), 1979, *Electromagnetic Interactions in Elastic Solids*, Springer Verlag, Wien, New York

20. RAO S.S., SUNAR M., 1993, Analysis of Distributed Thermopiezoelectric Sensors and Actuators in Advanced Intelligent Structures, *AIAA Journal*, **31**, 7, 1280-1286

21. SPORN D., SCHÖNECKER A., 1999, Composites with Piezoelectric Thin Fibers – First Evidence of Piezoelectric Behaviour, *Mat. Res. Innovat.*, **2**, 303-308

22. TIERSTEN H.F., 1969, *Linear Piezoelectric Plate Vibration*, Plenum Press, New York

23. TZOU H.S., ANDERSON G.L. (edit.), 1992, *Intelligent Structural Systems*, Kluwer Academic Publishers

24. TZOU H.S., 1993, *Piezoelectric Shells (Distributed Sensing and Control of Continua)*, Kluwer Academic Publishers, Dordrecht/Boston/London

25. TZOU H.S., YE R., 1994, Piezothermoelasticity and Precision Control of Piezoelectric Systems: Theory and Finite Element Analysis, *Journal of Vibration and Acoustics*, **116**, 489-495

26. TZOU H.S., GURAN A. (edit.), 1998, *Structronic Systems: Smart Structures, Devices and Systems, Part 1: Materials and Structures, Part 2: Systems and Control*, World Scientific

27. VOIGT W., 1910, *Lehrbuch der Kristallphysik*, Teubner, Leipzig

28. WEBER CH.-T., GABBERT U., SCHULZ I., 1998, Actuator Placement in Smart Structures by Discrete-Continuous Optimization, *Proceedings of the 4th European and 2nd MIMR Conference on Smart Materials and Structures*, Harrogate, UK, 475-484

Zastosowanie metody elementów skończonych do analizy i projektowania piezoelektrycznie sterowanych konstrukcji inteligentnych

Streszczenie

Praca daje przegląd nowych osiagnięć z zakresu modelowania, analizy numerycznej i projektowania konstrukcji inteligentnych z piezoelektrycznymi elementami wykonawczymi. Omówiono teoretyczne podstawy opracowanych przez autorów narzędzi symulacyjnych korzystających z metody elementów skończonych. Narzędzie to zawiera zarówno jedno-, dwu- i trójwymiarowe sprzężone elementy termo-elektromechaniczne, jak i elementy skończone nadajace się do symulacji statyki i dynamiki płyt i powłok warstwowych ze sterowaniem. Możliwe jest również włączenie algorytmów optymalizacyjnych, np. służących do optymalnego wyznaczania położenia aktuatora. Aktywnie sterowana belka, zagadnienie wibroizolacji pojemnika oraz wibroizolacji płyty jako części pobudzanej konstrukcji walcowej są przykładami pokazującymi możliwości i efektywność opracowanego narzędzia.

Manuscript received December 17, 1999; accepted for print January 21, 2000